Chemical and isotopic architecture of the belemnite rostrum

C.V. Ullmann[a,b,*], R. Frei[a], C. Korte[a], S.P. Hesselbo[b]

aUniversity of Copenhagen, Department of Geosciences and Natural Resource Management, Øster Voldgade 10, 1350 Copenhagen K, Denmark.
bUniversity of Exeter, Camborne School of Mines and Environment and Sustainability Institute, College of Engineering, Mathematics and Physical Sciences, Penryn Campus, Penryn, Cornwall TR10 9FE, UK.
*correspondence: c.v.ullmann@gmx.net; phone: +44 1326 255 721; fax: +44 1326 370 450

Abstract

Macrofossil calcite is of great importance for quantitative reconstructions of palaeoenvironment and palaeoseasonality. The calcite rostra of belemnites, Jurassic to Cretaceous marine invertebrates, are especially suited for such investigations, because they are comparatively large and are structured by growth bands. Despite their use in chemostratigraphic and palaeoenvironmental studies, much of the internal variability of geochemical signatures in rostra is poorly understood.

Here, multiple profiles through a belemnite rostrum of *Passaloteuthis bisulcata* (~183 Myr old) were analyzed for $\delta^{13}C$ and $\delta^{18}O$ values as well as Mg/Ca, Sr/Ca and Mn/Ca ratios. Geochemical signatures of the central 1-2 mm of the profiles indicate diagenetic cementation along the apical zone, for which original porosity of up to 40 % can be inferred. The overall $\delta^{13}C$ and $\delta^{18}O$ values of the other, well preserved parts of the belemnite fluctuate by > 1 per mil, but are nearly uniform within single growth bands. In contrast, Sr/Ca and Mg/Ca in the well-preserved parts show growth-rate and crystal-shape related variability. Close to the central apical zone, strongly bent calcite crystals are enriched in Mg (up to 70 %) and Sr (up to 50 %). Through the remainder of the rostrum, higher calcite precipitation rate can account for Mg depletion of ~15 % and Sr enrichment of ~15 % with respect to co-genetic calcite precipitated at a slower rate. No indication for temperature control on Mg/Ca or Sr/Ca is detected in the investigated specimen. Overall, the new findings indicate that $\delta^{13}C$ and $\delta^{18}O$ analyses of belemnite rostra produce consistent results regardless of the sampling area within the rostrum, and that growth rate effects on element incorporation are minor with respect to the control exerted by secular changes in seawater composition through time. Additionally, the central part of the rostrum, where strong calcite crystal bending is observed, should be avoided for sampling when studying elemental composition of the calcite for palaeoenvironmental reconstructions.

1 INTRODUCTION

Belemnite fossils have played a key role ever since fossil calcite was first identified as a promising archive for geochemical studies of past environmental conditions (e.g. **Urey et al., 1951**; **Stevens and Clayton, 1971**; **Sælen et al., 1996**; **McArthur et al., 2000, 2007**; **Bailey et al., 2003**; **Rosales et al., 2004a**; **Wierzbowski and Joachimski, 2007**; **Price and Rogov, 2009**; **Nunn and Price, 2010**; **Wierzbowski and Rogov, 2011**; **Zakharov et al., 2011**; **Price and Passey, 2013**; **Ullmann et al., 2013a,b, 2014**). The belemnite rostrum has been extensively investigated and is thought to be composed originally of calcite containing variable amounts of organic matter (**Sælen, 1989**; **Fuchs, 2012**). Detailed investigation of the growth bands within belemnite rostra, as well as comparisons to modern analogues suggest a belemnite life cycle of a few years at maximum (**Rexfort and Mutterlose, 2006**; **Wierzbowski and Joachimski, 2009**; **Wierzbowski, 2013**); thus seasonal changes in environmental parameters can be recorded in the calcite. High resolution studies of single rostra have been conducted to derive information about seasonal temperature variability (**Urey et al., 1951**; **Longinelli, 1969**; **Stevens and Clayton, 1971**; **Zakharov et al., 2011**).

The variability of all geochemical proxies in the rostrum leads to considerable data spread within chemostratigraphic records derived from belemnite fossils (**McArthur et al., 2000**; **Bailey et al., 2003**; **Price and Rogov, 2009**; **Dera et al., 2011**; **Ullmann et al., 2013b, 2014**). The causes for this heterogeneity are not very well constrained but are of much importance for better understanding past environments. Besides diagenesis, environmental parameters such as seawater composition and temperature, metabolic and taxon-specific effects, as well as calcite precipitation rate, might play variably important roles in determining how each geochemical proxy is represented within rostra. Potential contributions of these parameters have been explored in a series of studies (**Rosales et al., 2004b**; **Dutton et al., 2007**; **McArthur et al., 2007**; **Wierzbowski and Joachimski, 2009**; **Li et al., 2012, 2013**), occasionally combining isotopic and elemental proxies. Comprehensive datasets for multiple, complete profiles through belemnite rostra are, however, lacking.

Here we report high resolution $\delta^{13}C$ and $\delta^{18}O$ data as well as Mg/Ca, Sr/Ca, and Mn/Ca ratios for four comparable and complete transects through a single rostrum of *Passaloteuthis bisulcata* (Early Toarcian, Yorkshire, UK). The analytical results are discussed in terms of robustness of geochemical proxies within a rostrum and the extent to which crystal morphology and calcite precipitation rate can affect skeletal chemistry.
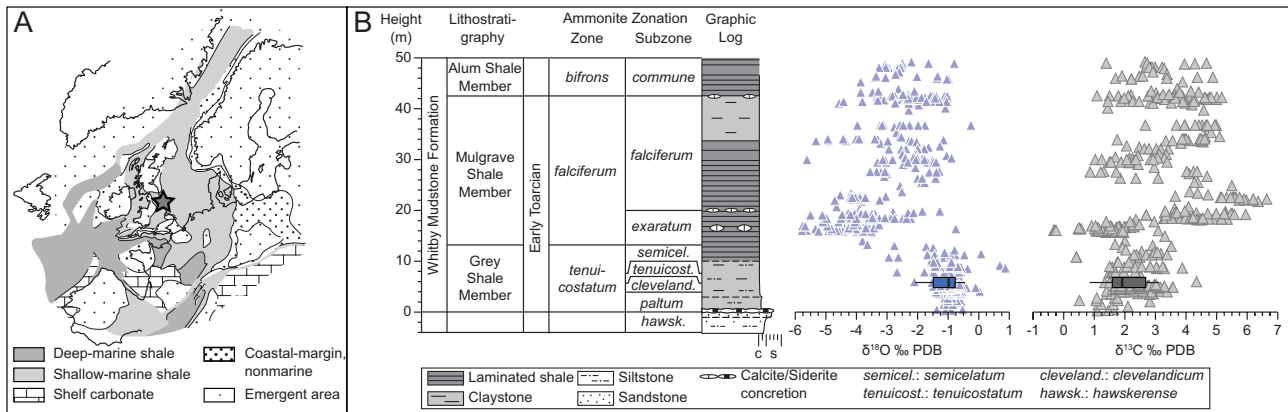
Fig. 1: A: Palaeogeography of Europe during the Early Jurassic (modified from **Coward et al., 2003**) with star indicating sample locality. B: Simplified lithology and belemnite chemostratigraphy of the Early Toarcian in the Cleveland Basin. The box plots show results obtained for the specimen investigated in the present study. The box encompasses the second and third quartile with the median as black line and the whiskers show the ranges from the 2.5 to 97.5 percentile (n = 324). Chemostratigraphic data are from **Sælen et al. (1996)**, **McArthur et al. (2000)**, **Li et al. (2012)** and **Ullmann et al. (2014)**.

2 MATERIALS AND METHODS

2.1 Belemnite specimen

A rostrum of *Passaloteuthis bisulcata* (Blainville), collected at Hawsker Bottoms (Yorkshire, UK), has been analysed in the present study (**Fig. 1,2**). This specimen was chosen, because it originates from a lithologically, biostratigraphically, and chemostratigraphically well-studied succession, stems from a time interval of relative environmental stability and was found in almost complete state, allowing for determination to species level. The sample originates from the Grey Shale Member, 67 cm above the base of the *Dactylioceras tenuicostatum* Subzone of the *Dactylioceras tenuicostatum* Zone, Early Toarcian, Jurassic (**Hesselbo and Jenkyns, 1995**). Continuous microsampling was undertaken via four transects through the rostrum using a handheld drill (**Fig. 3a,d**). The transects were positioned from close to the proto-conch (profile one) towards the apex (profiles two to four)
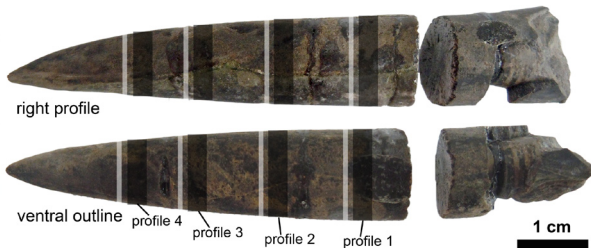

Fig. 2: Specimen of *Passaloteuthis bisulcata* investigated in this study. Locations of sampled profiles are indicated as dark bands and associated thick sections taken for cathodoluminescence analyses and photographs as pale bands.

and were oriented slightly oblique to the ventral-dorsal axis to avoid sampling cracks which might be associated with diagenetic alteration (**Fig 3a,b, 4**). The placement of the profiles was chosen to sample the same number of growth increments on the ventral and dorsal side multiple times with different increment thicknesses (**Fig. 3c**). Average spatial resolution along these profiles is ~0.11 mm per sample. Profiles two to four yield consecutively fewer growth bands, and the growth bands present become thicker towards the apex due to the geometry of the belemnite rostrum (**Fig. 3a,c**). In order to ascertain diagenetic effects on the geochemical signatures in the belemnite rostrum, alveolar calcite cement was chosen for analysis (see **Sælen et al., 1996** for a similar approach).

The alveolus of the specimen selected for detailed geochemical analysis was filled with silty sediment rather than pure calcite. Therefore, analytical results from this specimen of *P. bisulcata* are compared to isotope and element measurements of 23 calcite cement samples from the alveolar area of another specimen of *Passaloteuthis* sp. originating from 44 cm lower in the same succession.
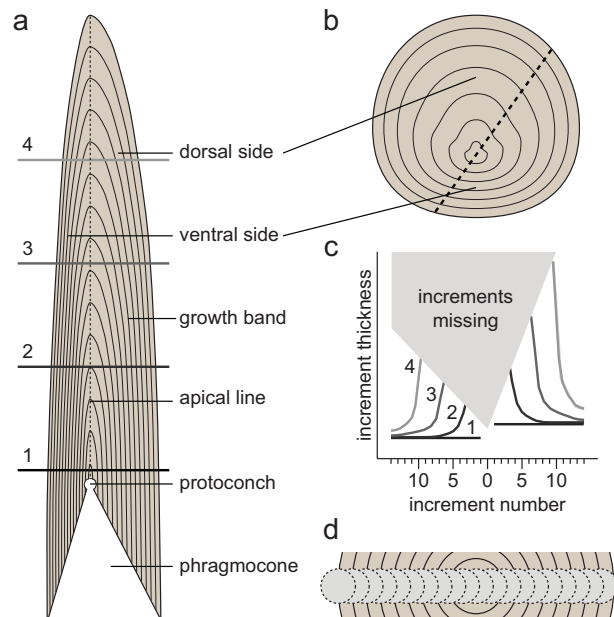

Fig. 3: a) Schematized lateral section of *Passaloteuthis* with terminology of the structural features. The numbered lines indicate approximate position of the profiles analyzed. b) Schematized cross section of *Passaloteuthis* indicating the approximate position of transects analyzed. c) Relative thickness of increments within the rostrum. The increments on the ventral side are narrower than those of the dorsal side due to asymmetry of the rostrum. Towards the apex of the rostrum, progressively more growth bands representing early growth stages of the belemnite are missing. Due to the morphology of the rostrum growth bands are relatively thickest at the apical line and apex. d) Sampling of the belemnite profiles. The belemnite samples were taken via progressive drilling starting from the ventral margin of each section.

2.2 Analytical methods

The rostrum was sawn into slabs of ~4 mm thickness oriented perpendicular to the apical line. These slabs were fixed on glass plates using epoxy resin. After curing of the resin, the slabs were lapped down to ~3.5 mm
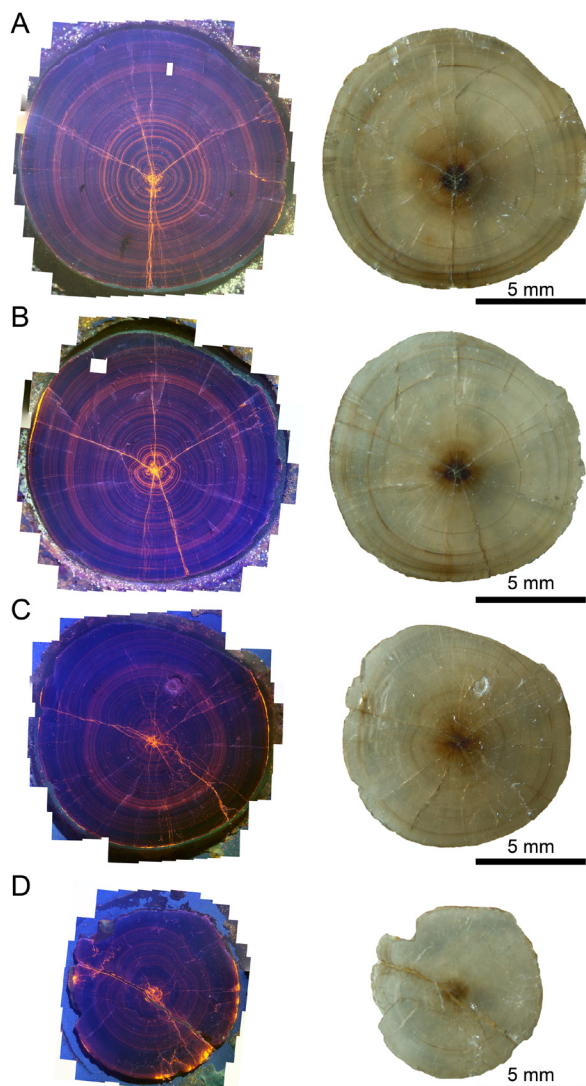
Fig. 4: Cathodoluminescence images (left) and photographs (right) of sections analyzed in this study. A: Profile one; B: Profile two; C: Profile three; D: Profile four. The cathodoluminescence images and photographs were taken after sampling for geochemical proxies and lapping the slabs down to ~500 μm thickness. Small damages at the lower left rim (A-C and in the central upper part of C were induced during the sampling).

thickness and hand-polished using 400 and 1000 mesh silicon carbide powder and 1200-4000 mesh sandpaper. Calcite samples of ~0.6 mg were drilled out of the calcite slabs and transferred into 3.5 ml glass vials for analysis of $\delta^{13}C$ and $\delta^{18}O$ values. The transects through the fossil material were prepared such that the lower ~0.5 mm of the section remained intact. After completion of the sampling for geochemical analyses, the calcite slabs were lapped down to ~500 μm thickness and polished for later microscopic and cathodoluminescence inspection (**Fig. 4**). Cold-cathode luminescence petrography was carried out using a Citl Mk-3a electron source at the University of Exter Camborne School of Mines, operated at approximately 350 μA and 10 kV, and observed using a Nikon digital camera at a spatial resolution of ~1.5 μm per pixel and with a 4 second exposure time.

Carbon and oxygen isotope ratios were measured using an IsoPrime Gas Source Isotope Ratio Mass Spectrometer at the University of Copenhagen. Analytical procedures for stable isotope analyses are the same as described in **Ullmann et al. (2013a)**, adopting routines for continuous flow measurements following **Spötl and**

Vennemann (2003) with some modifications owing to laboratory infrastructure. Accuracy of the analyses was controlled by multiple measurements of NIST SRMs 8543 and 8544. The Copenhagen in-house reference material LEO (Carrara Marble: $\delta^{13}C$ = +1.96 ‰; $\delta^{18}O$ = -1.93 ‰) reproduced within 0.10 ‰ for $\delta^{13}C$ and 0.15 ‰ for $\delta^{18}O$ (2 sd, n = 102) during the course of the measurements.

Phosphoric acid solutions of samples remaining after stable isotope analyses were further processed for measurements of element/Ca ratios (**Coleman et al., 1989**). Analytical details are given in the Supplementary Information of **Ullmann et al. (2014)**. Briefly, samples were diluted to a nominal Ca concentration of 25 μg/g and measured against a set of matrix matched calibration solutions using an Optima 7000 DV ICP-OES at University of Copenhagen. Measurement repeatability was assessed by multiple measurements of the limestone reference material JLs-1 (**Imai et al., 1996**), yielding a Mg/Ca ratio of 14.0 ± 0.3 mmol/mol, a Sr/Ca ratio of 0.343 ± 0.007 mmol/mol and Mn/Ca ratio of 0.03 ± 0.03 mmol/mol (2 sd, n = 68). Reproducibility of Mn/Ca ratios at low Mn concentrations was limited due to transient memory effects on the ICP-OES. Analytical uncertainty is estimated to be around ± 0.03 mmol/mol for the whole range of Mn/Ca ratios observed in the fossil specimens and about 3 % for the higher values measured in the calcite cement (**Ullmann et al., 2013a**). Reproducibility (2 rsd) of Mg/Ca ratios and Sr/Ca ratios calculated from multiple measurements of JLs-1 is 2.1 % and 1.9 %, respectively.

3 RESULTS

3.1 Belemnite structure and texture

The belemnite slabs are generally pale brown in colour and translucent, with some growth bands standing out as darker or paler bands (**Fig. 4**). The apical line is displaced from the geometrical centre of the sections towards the ventral side, making the dorsal region slightly thicker than the ventral region (**Fig. 3a,b**). The central ~2 mm of each slab are visibly darker than the surrounding (**Fig. 4**). Each slab shows multiple fractures that all meet at the apical line. Under cathodal excitation, most of the calcite of the rostrum is characterized by blue 'intrinsic' luminescence, and a multitude of growth bands that show dull violet to orange luminescence (**Fig. 4**). Rims, fractures and the central apical zone instead show bright orange to yellow luminescence. The two well-developed dorso-lateral grooves characteristic of *Passaloteuthis* (**Doyle, 1990**) are visible as depressions in the central growth bands especially in the cathodoluminescence image of profile 2 (**Fig. 4b**). In the three sections closest to the protoconch (**Fig. 3a, 4**), fractures run through both traces of the grooves, whereas in the section closest to the apex only one such fracture is observed. A small fraction of the right dorsal region of the rostrum is missing in all sections (**Fig. 4**) either due to physical abrasion or chemical corrosion during exposure on the wave-cut platform of the outcropping succession.

3.2 Geochemical results of transects

All four geochemical profiles are nearly symmetrical

about the apical line, showing systematic fluctuations of the measured parameters (**Fig. 5**, **Appendix 1**). In general, δ¹³C values range from +0.4 to +3.3 ‰ and δ¹⁸O values from -2.7 to -0.3 ‰, but parallel decreases to as low as -2.3 in δ¹³C and -5.8 ‰ in δ¹⁸O, are observed at the apical line. Minimum Mg/Ca ratios in the four profiles are similar and between 6.8 to 7.3 mmol/mol. Maximum Mg/Ca ratios, which occur near the apical line, however, increase from profile one (11.8 mmol/mol) to profile four (18.1 mmol/mol). At the apical line, inconsistent behaviour of Mg, trending downwards in profiles one and four, upwards in profile two and remaining stable in profile three, is noted. Both, minimum Sr/Ca ratios (1.27-1.54 mmol/mol) and maximum Sr/Ca ratios (1.86-2.20 mmol/mol) increase from profile one to profile four. In all four cases, Sr/Ca ratios drop significantly at the apical line, but the magnitude of the decrease diminishes from profile one towards profile four from ~0.6 mmol/mol to 0.3

mmol/mol (**Fig. 5**). Mn/Ca ratios in all four profiles show a peak at the apical line and a secondary enrichment at the ventral margin. Maximum Mn/Ca ratios are significantly higher in the first two profiles (0.73 and 0.83 mmol/mol) compared to profiles three and four (0.47 and 0.43 mmol/mol). In profile four an additional slight Mn enrichment in the dorsal part reaching 0.11 mmol/mol at most is observed (**Fig. 5**).

The systematic fluctuations of carbon isotope ratios in profile one allow for the allocation of a series of isotopic spikes that can be seen on either side of the apical line. From the inner growth bands to the margins a set of five negative and five positive carbon isotope spikes is indicated (**Fig. 5**). Carbon isotope spike V+ is missing on the dorsal part of the profile due to the abrasion of the marginal part of the rostrum. In the profiles two to four, more and more carbon isotope spikes of the inner growth bands are missing (representing the earlier
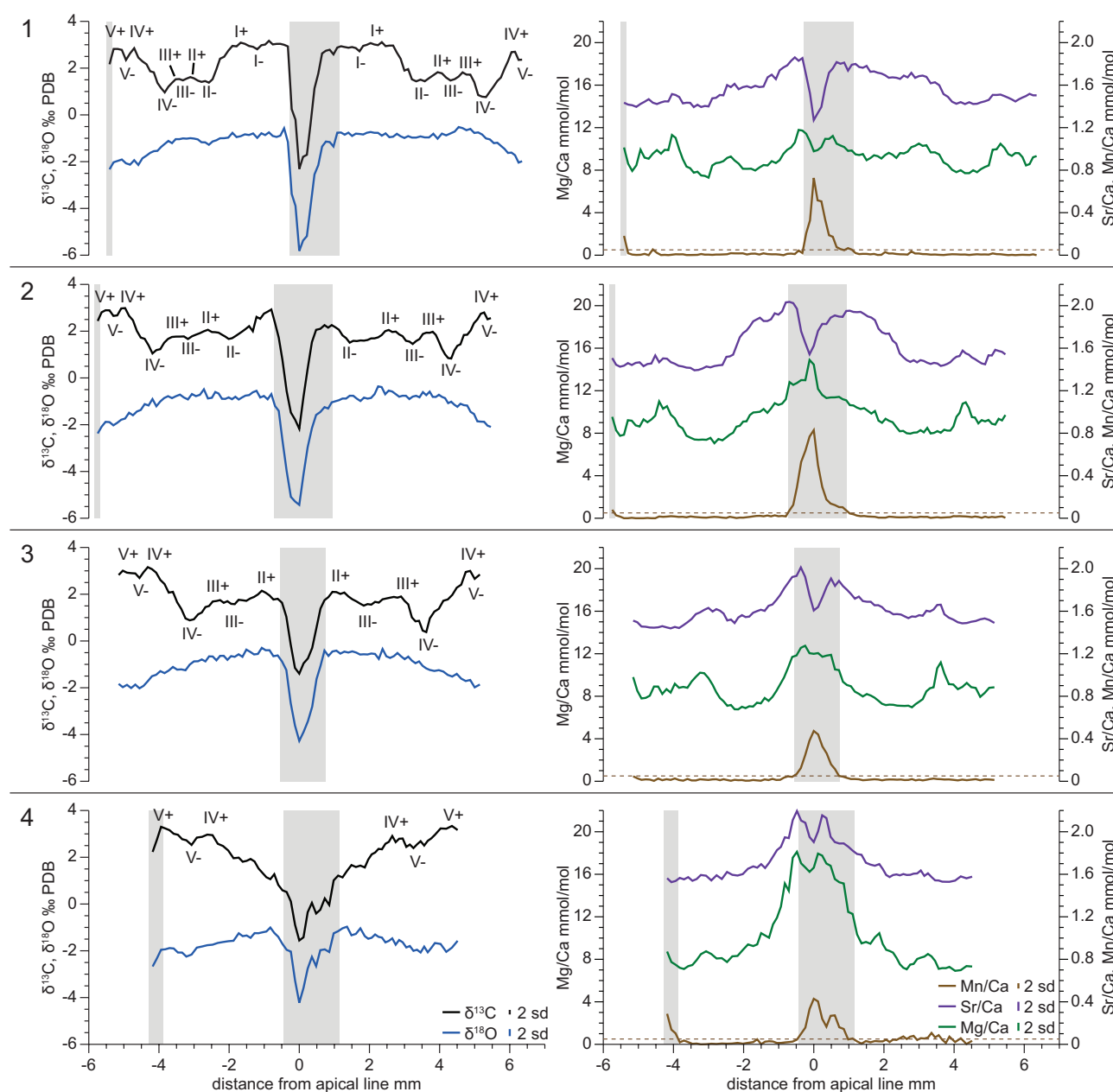

Fig. 5: Geochemical results for the four profiles through the specimen of *Passaloteuthis bisulcata*. Approximate positions of the profiles are indicated in **Fig. 3a**. Spikes in the carbon isotope profiles in profile one are labelled from the earlier growth stages to the later growth stages and correlated to the other three profiles. The maximum accepted Mn/Ca ratio for well-preserved sample material of 0.05 mmol/mol is plotted as stippled line. Grey vertical bands mark parts of the profiles that are considered affected by alteration. 2 sd uncertainties for element ratios scale with the measured value and are here shown for the respective maximum measured ratios.

growth stages of the belemnite, **Fig. 3a**). Profile two lacks carbon isotope spikes I- and I+; profile three additionally lacks II- and in profile four only the outermost three carbon isotope spikes are recognized. The spacing between the carbon isotope spikes gradually increases from profile one towards profile four. Similar features can be observed for the other geochemical tracers, apart from Mn/Ca, whose significant enrichment is restricted to the central ~1.5 mm of each profile.

Isotope ratios of the diagenetic calcite cement span a narrow field from -10.1 to -8.9 ‰ with a median of -9.9 ‰ in the case of carbon, and -14.8 to -12.6 ‰ with a median of -14.5 ‰ in the case of oxygen (**Fig. 6**). The Mg/Ca ratios range from 13.4 to 22.0 mmol/mol with a median of 19.9 mmol/mol and Sr/Ca from 1.11 to 1.61 mmol/mol with a median of 1.45 mmol/mol. The Mn/Ca ratios are relatively uniform and fall into the interval of 4.07 to 4.62 mmol/mol with a median of 4.38 mmol/mol. Heaviest $\delta^{18}O$ values in the cement are associated with lowest Mg/Ca and Sr/Ca ratios as well as highest $\delta^{13}C$ values and Mn/Ca ratios (**Fig. 6**).
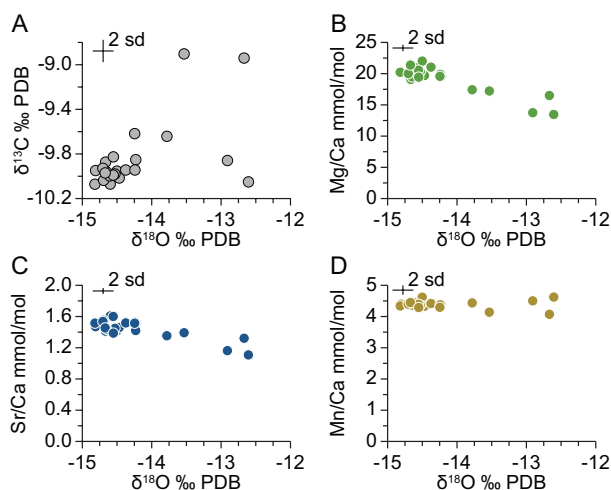

Fig. 6: Geochemical data for calcite cement in alveolar infill of the fragment of *Passaloteuthis* sp. sampled 44 cm below the specimen analyzed in this study. Most of the data cluster at low $\delta^{18}O$ values.

4 DISCUSSION

4.1 Diagenetic alteration

Diagenesis can erase the palaeoenvironmental information from macrofossil shells (see **Ullmann and Korte, 2015** for a recent review). Samples must therefore be assessed for diagenesis when using geochemistry for palaeoclimatic and/or palaeoecological reconstruction. Qualitative geochemical trends of alteration are well established (**Brand and Veizer, 1980, 1981**; **Al-Aasm and Veizer, 1986a,b**), predicting bright orange luminescence under cathodic excitation, decreasing $\delta^{13}C$, $\delta^{18}O$ and Sr/Ca, and increasing Mn/Ca with progressive alteration. Isotopic ratios are most often the target of environmental interpretation. It is therefore difficult to use $\delta^{18}O$ and $\delta^{13}C$ independently for identifying altered samples. A routine application of Sr/Ca ratios for detecting diagenetic imprints in biogenic calcite is also problematic because the original composition of the fossil is taxon specific, and can be variable within single fossils, and through geological time (**Korte and Hesselbo, 2011**; **Li et al., 2012**;

Ullmann et al., 2013b; **Ullmann and Korte, 2015**). The Mn/Ca ratio is the most widely employed alteration maker because Mn levels in primary shell material are usually very low, while diagenesis leads to Mn enrichment (**Veizer, 1974**; **Brand and Veizer, 1980**; **Al-Aasm and Veizer, 1986a**). Most of the profiled sections show intrinsic luminosity and dull luminescent growth bands and the luminescence of these growth bands is most likely related to the presence of traces of Mn (e.g. **Machel, 1985**; **Barbin, 2000**; **Benito and Reolid, 2012**). These enrichments, if related to diagenetic effects on the calcite of the rostrum, are too small to cause any measurable difference to the analyzed geochemical proxies: a Mn/Ca ratio of 0.05 mmol/mol corresponds to the Mn level at which diagenetic effects on oxygen isotopes reach a magnitude equal to analytical reproducibility, assuming that the geochemical signatures of the calcite cement are representative of the diagenetic signal. We therefore adopt this Mn/Ca ratio for the maximum acceptable degree of alteration. Variable critical upper limits of Mn/Ca for acceptable degree of alteration are employed (**Bailey et al., 2003**; **Nunn and Price, 2010**; **Korte and Hesselbo, 2011**; **Ullmann et al., 2013a,b, 2014**; **Ullmann and Korte, 2015**), owing to variable physicochemical conditions during alteration (**Ullmann et al., 2013a**). The value of 0.05 mmol/mol adopted here falls in the lower end of applied limits (see table 1 in **Ullmann and Korte, 2015**). The elemental and isotopic data of 12 samples from the dorsal side of profile four that exceed this Mn limit were considered in the following discussion because they do not show significant offset from those data derived for the ventral side of this profile where Mn/Ca ratios are consistently lower than 0.05 mmol/mol.

The margins and apical zone of all sections show bright orange to yellow luminescence (**Fig. 4**), indicating that here diagenetic overprint is significant. Samples that are excluded on the basis of elevated Mn/Ca ratios are located in the same regions; the central 1.4 to 1.8 mm around the apical line, and six samples originating from the ventral margin of the specimen. Preferential alteration is described for areas around the apical line and the rim (**Podlaha et al., 1998**; **McArthur et al., 2000, 2007**; **Ullmann et al., 2013a**) suggesting that our observations are representative for belemnite rostra in general. The $\delta^{13}C$ and $\delta^{18}O$ values in the central parts of the profiles are strongly positively correlated (r^2 of 0.95 to 0.99) and trend towards a composition compatible with the calcite cement (**Fig. 7**). With respect to isotopic composition, these diagenetically altered areas of the rostrum can therefore be described by a binary mixing between the calcite cement and primary shell calcite. Such a simple relationship is best explained by variable degrees of cementation of an originally partially porous apical line (see also **Veizer, 1974**; **Spaeth, 1975**). Were the calcite additionally affected by dissolution and re-precipitation phenomena, more variability of the isotope data would be expected. Assuming the median $\delta^{13}C$ value of -9.95 ‰ as representative for the calcite cement and the respective most positive $\delta^{13}C$ adjacent to each diagenetically altered section as the end member composition for the primary shell material (+1.1 to +2.9 ‰ depending on the profile; see **Fig. 5**), degrees of cementation can be computed. The
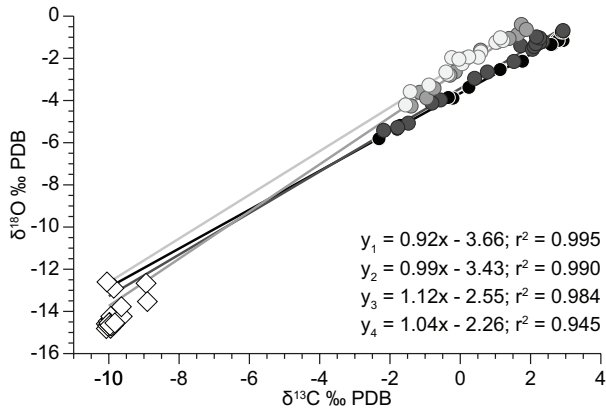
Fig. 7: Cross plot of δ¹³C and δ¹⁸O values in the calcite cement (white diamonds) and the apical segment of the profiles (circles) interpreted to be affected by post-depositional overprint (darkest: profile one; palest: profile four). Very strong linear correlations trending towards isotopic ratios compatible with the calcite cement are observed for all four profiles.

respective maximum degrees of cementation are 41 % for profile one, 40 % for profile two, 28 % for profile three and 24 % for profile four. These findings suggest that the apical zone of rostra of *P. bisulcata* was originally slightly porous, with a maximum porosity of ~40 % at the apical line close to the protoconch. No indication for such porosity further than ~0.9 mm away from the apical line is observed, indicating that in the later growth stage, precipitates were originally massive calcite. In the central area of the profiles, Sr/Ca ratios and Mn/Ca ratios also display strong linear correlations with δ¹⁸O values in most cases, but correlation coefficients are generally lower and extrapolations of the linear trends are not always compatible with the composition of the calcite cement. These findings imply that the diagenetic response of trace elements is more complicated, e.g. due to locally variable supply of Mn to the diagenetic fluid (**Ullmann et al., 2013a**) and calcite precipitation rate (**Rimstidt et al., 1998; DePaolo, 2011**).

4.2 Reproducibility of geochemical proxies within belemnite rostra

If growth bands constitute original features of biomineralization and the primary signatures of the rostrum are preserved, the geochemical proxies within each profile should show the same trends in the ventral and the dorsal side of the rostrum. To test this hypothesis, the dorsal and the ventral side were superimposed for all profiles. For each profile a diameter of the original profile, including the missing dorsal margin, was assumed (**Table 1**). The absolute position of each sample point on the profile was subsequently normalized such that the margin was assigned the value one and the apical line the value zero (**Fig. 8**). It can be assumed that between 4 and 12 % of the dorsal part of the profiles is missing, and that towards the

Table 1: Geometry of the profiles and empirical parameters used for superposition of geochemical data.

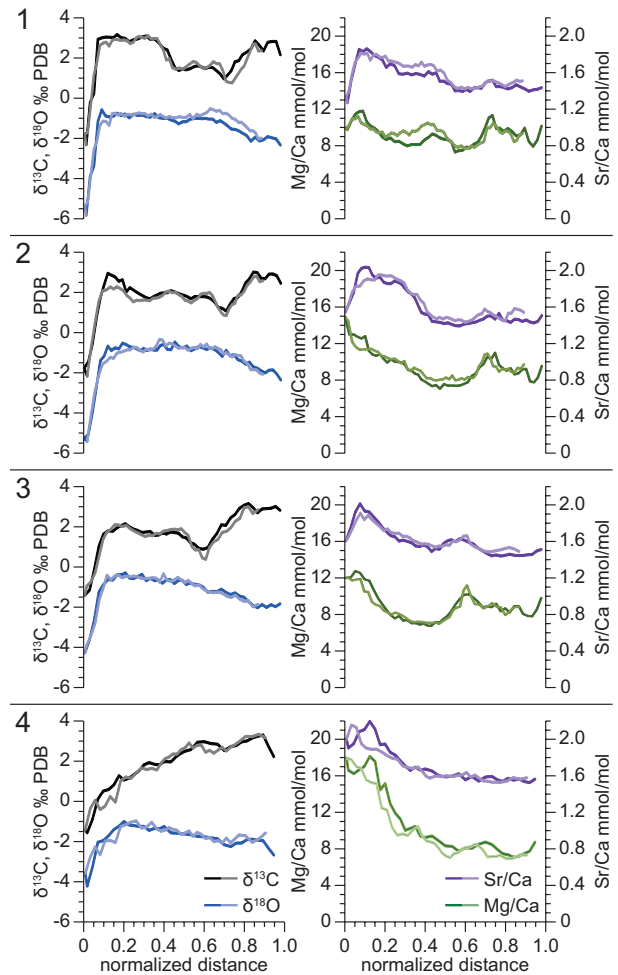| profile number	diameter	position of center	c1	c2
	mm	mm		
1	12.7	5.60		
2	12.0	5.75	0.33	1.11
3	11.2	5.30	0.48	0.70
4	9.4	4.50	0.70	0.34

Fig. 8: Superposition of ventral (darker) and dorsal (paler) parts of the four geochemical profiles. The x-axes are normalized such that the apical line has the value of zero and the margin the value of one.

apex of the rostrum preservation is progressively more complete. Superposition of the two half-profiles shows an excellent fit of the geochemical signatures, evidencing a very good preservation of the material and robustness of the data within the section (**Fig. 8**).

It is of interest to assess, whether the geochemical proxies of each growth band give comparable results throughout the entire belemnite rostrum. In order to allow for the comparison of the four profiles, age models for the individual transects have to be constructed. As shown in **Figure 3c**, the thickness of each growth increment is greater on the dorsal side than on the ventral side due to the slightly asymmetric growth of the rostrum. Furthermore, more and more growth bands representing the younger life stages of the belemnite are missing the further away from the protoconch the profile is laid. Lastly, again due to the geometry of the growth bands, increments decrease in thickness away from the apex, with the growth bands representing the earliest life stage being the most expanded (**Fig. 3a,c, 9**). While the asymmetry of the ventral versus dorsal side was accounted for when normalizing and superposing both halves of each profile, the progressive loss of growth bands and non-linear expansion have to be addressed. The cathodoluminescence images of the associated sections can help to correlate the geochemical signatures of the profiles. While these images were of necessity taken slightly offset from the geochemical profiles (**Fig. 2**), they enable construction of a mathematical model for the geometry
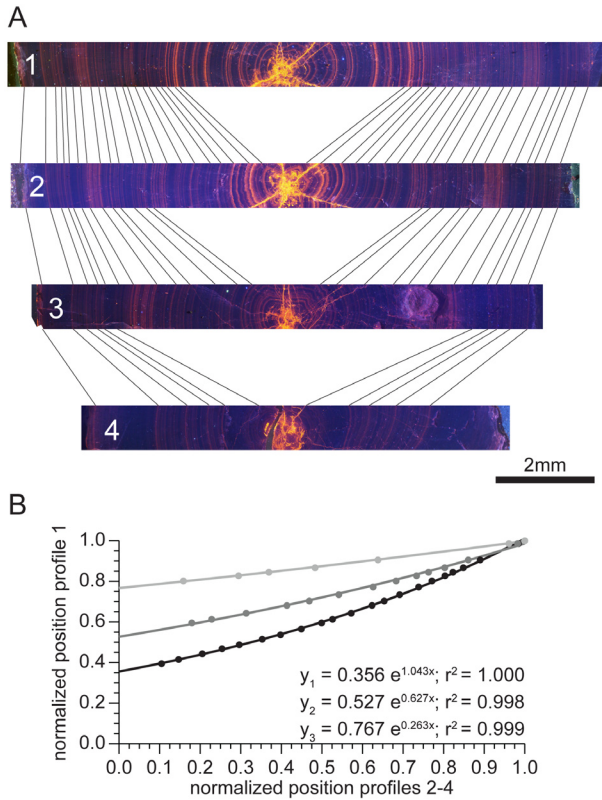
Fig. 9: A: Cathodoluminescence images corresponding to the geochemical profiles. The outermost luminescent bands can be traced and correlated through all four profiles, whereas more and more of the central bands are missing towards profile four. B: Cross plot of the normalized position of the growth bands correlated from A in profile one versus the other profiles (black circles: profile two; dark grey circles: profile 3; light grey circles: profile 4). 0 corresponds to the apical line and 1 to the rim. Numerical values and correlation coefficients for exponential trend lines are given as y_1 (profile 2), y_2 (profile 3), y_3 (profile 4).

In figure B:
$y_1 = 0.356\ e^{1.043x}$; $r^2 = 1.000$
$y_2 = 0.527\ e^{0.627x}$; $r^2 = 0.998$
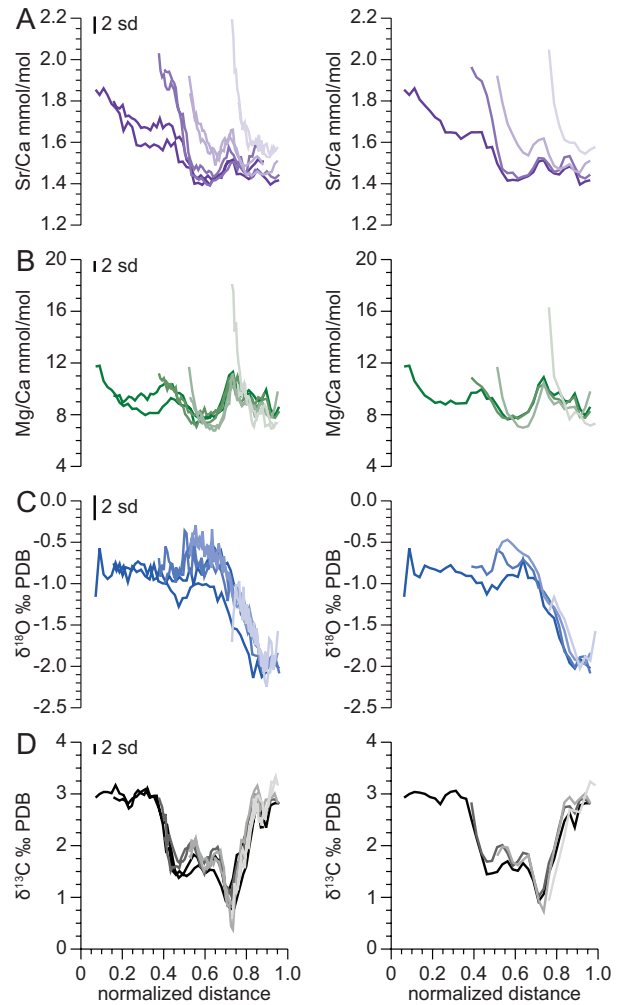$y_3 = 0.767\ e^{0.263x}$; $r^2 = 0.999$

Fig. 10: Superposition of the well-preserved parts of the four geochemical profiles (profile one darkest; profile four palest colours). Sample positions within profiles two to four are corrected for changes in growth increment thickness and missing growth bands towards the apical line. Left side: all data; right side: data for each profile binned in 0.025 intervals of normalized distance.

of the growth bands and yield approximate values for matching the profiles (**Fig. 9**). Band-by-band correlation of the cathodoluminescence images (**Fig. 9a**) can be used to plot the relative position of each growth band in the profiles (**Fig. 9b**). This cross plot of the normalized position of the growth bands in profile versus the other profiles shows a relationship that can best be approximated by an exponential function of the form:

$$f_{corr} = c_1 * \exp(c_2 * f_{norm})$$

with f_{corr} as the corrected normalized position of each sample; c_1 as the y-axis intercept in **Fig. 9b** predicting the fraction of the profile missing from profiles two to four (0: the section is as complete as profile one; 1: none of the growth bands from profile one is present); c_2 scaling the curvature of the calibration function; fnorm as the normalized position of the sample as shown in **Fig. 8**. Empirically fitted values for c_1 and c_2 are shown in **Table 1** and closely match the values predicted from the slightly offset cathodoluminescence slides. Deviations are towards lower values of c_1 because the analyzed profiles are further away from the apex than the respective cathodoluminescence image and thus comprise a more complete set of growth bands (**Fig. 2, 3**). Deviations increase from profile two to profile four due to the increasing curvature of the specimen towards the apex (**Fig. 2, 3**).

The superposition of the four profiles excluding the part identified as altered is shown in **Figure 10**, with all analytical results on the left side and binned in 2.5 % steps on the right side. A very good agreement of the four profiles is seen for carbon and oxygen isotope ratios, with discrepancies generally below 0.5 ‰. For Mg/Ca and Sr/Ca, the profiles show the same patterns towards the margin of the rostrum, but deviate significantly in absolute values. A strong increase of both, Mg/Ca and Sr/Ca towards the apical line is seen in all four profiles, affecting circa the central 4 mm of each profile. These increases amount to a maximum of ca. 70 % for Mg/Ca in profile four over the reference value from profile one and to 50 % for Sr/Ca, also in profile four. Furthermore, a relative decrease of Mg/Ca ratios within a given growth increment is observed from profile one towards profile four, whereas the opposite is seen for Sr/Ca (**Fig. 10**). These offsets are smaller than the increases towards the centre of the rostrum and amount to ca. 15 % lower Mg/Ca and 15 % higher Sr/Ca in profile four than in profile one.

4.3 Structural interpretation

Because the same growth bands are transected up to eight times by the four profiles, effects of calcite structure and precipitation rate can be addressed. The belemnite rostrum is thought to be constructed from calcite crystals that originate from the apical line and grow perpendicular to the growth bands (**Sælen, 1989**; **Richter et**

al., 2011; Benito and Reolid, 2012). In *P. bisulcata* the calcite crystal surfaces are almost parallel to the apical line in the centre of the rostrum due to the rounded shape of the growth bands and then gradually bend towards a direction almost perpendicular to the apical line over the course of a few millimetres (Fig. 11, 12; see also Fig. 3a in Benito and Reolid (2012)). It is the zone where the crystal surfaces significantly change orientation that a strong enrichment of Mg and Sr in the calcite is observed in all four profiles. A similar pattern of Sr and Mg enrichment towards the apical line can be deduced from data obtained for *Acrocoelites subtenuis* in McArthur et al. (2007) and for *Cylindroteuthis puzosiana* in Li et al. (2013). We therefore interpret these strong element enrichments that are likely related to the distortions of the calcite crystals close to the apical line to be a common feature in belemnite rostra.
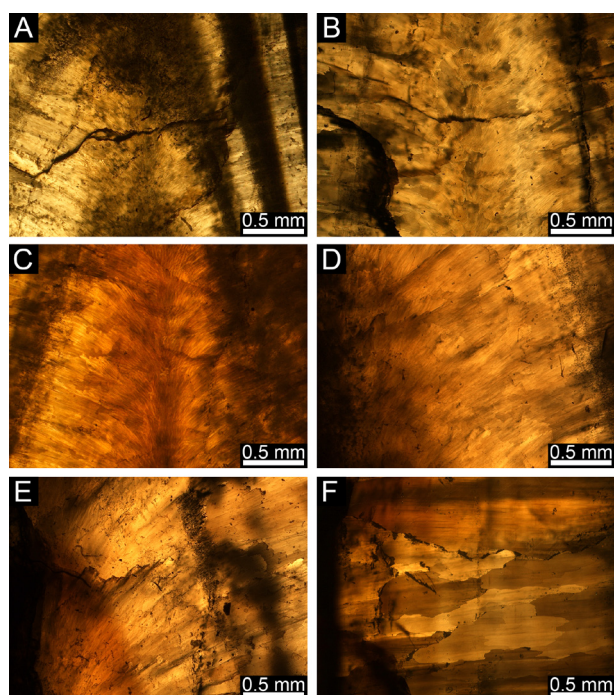
Fig. 11: Photomicrographs of thick sections (300-600 μm) taken under cross polarized light, showing the curved calcite morphology of the apical zone in different belemnite rostra from the Cleveland Basin (Yorkshire, UK). All images show the apical line in vertical orientation and the apex of the rostrum towards the top. A: Unidentified Toarcian belemnite rostrum. Very dark bands on the right side are growth bands. B: apical zone of Early Toarcian *Acrocoelites* sp. under cross polarized light. C: Unidentified Pliensbachian rostrum. D: *Passaloteuthis* sp. from the Early Toarcian *Dactylioceras tenuicostatum* Subzone. The apical line is on the left margin of the image. E: *Passaloteuthis* sp. from the earliest Toarcian *Protogrammoceras paltum* Subzone. The apical line is on the left margin of the image. F: Same specimen as E, showing crystal orientation perpendicular to the apical line and growth bands towards the margin of the rostrum. The apical line is ~5 mm to the left of the left margin. The patchy domains of differing extinction delineate crystal bundles of similar crystallographic orientation.

Further away from the apical line, other controls on the element proxies seem to prevail, as is evident from the parallel trends observed in all four profiles. Offsets of Mg/Ca and Sr/Ca between the four profiles are here not in the same direction as close to the apical line, but show opposing signs and are also less dramatic. The most prominent difference between the four profiles is the rate at which coeval calcite formation took place, with the relatively lowest rate encountered at profile one close to
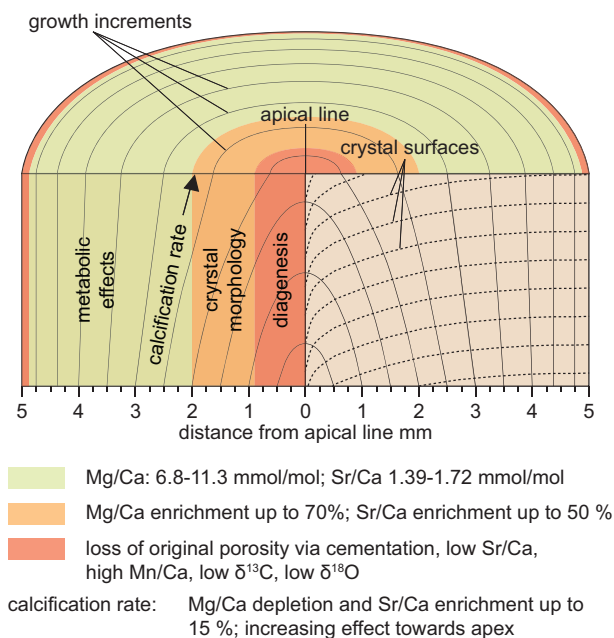
Fig. 12: Summary of structural and geochemical patterns observed in *P. bisulcata* on a schematized section through the rostrum. Parameters exerting significant control on the geochemical signatures and their approximate spatial extent are given on the left side of the scheme.

the protoconch, and the highest rate at profile four closest to the apex. The most likely effect generating the offset between the Sr/Ca and Mg/Ca profiles is therefore the calcite precipitation rate, with higher calcification rates leading to the incorporation of more Sr and less Mg than in the reference profile closest to the protoconch (Fig. 10). Relative changes in the distribution coefficients of Mg and Sr compatible with our observations have theoretical and experimental foundation: increases in Sr concentration due to higher calcite precipitation rate is compatible with geochemical models and experimental data (Morse and Bender, 1990; DePaolo, 2011; Gabitov et al., 2014), whereas for Mg, indication for the inverse has been found recently (Gabitov et al., 2014).

The general trace element patterns within each profile, excluding the part of the section which is influenced by calcite distortion, is such that Mg/Ca and Sr/Ca fluctuations are broadly parallel and more pronounced in Mg/Ca than in Sr/Ca. The overall range of Mg/Ca ratios in these parts of the profiles is from 6.8 to 11.3 mmol/mol (66 % variability), whereas that for Sr/Ca is from 1.39 to 1.72 mmol/mol (24 % variability). The dissimilar magnitude of variability between the two proxies and the parallel nature of their fluctuations rule out that lattice distortions or calcite formation rate are the driving processes defining their variability. The degree of variability especially of the Mg/Ca ratios further rules out that changes in ambient water composition can account for the observed ontogenetic trends. These considerations leave metabolic effects on element ratios in the mineralizing fluid as the most likely source for the documented data variability.

4.4 Fidelity of geochemical signatures

While the geochemical trends documented in the present study strictly only apply to a single belemnite specimen, some general conclusions for the interpretation of geochemical proxies from rostral calcite can be drawn that may be further substantiated through subsequent research (Fig. 12). Carbon and oxygen isotope ra-

tios in the four profiles show systematic fluctuations that agree within ~0.5 ‰ (**Fig. 10**), certifying the reliability of $\delta^{13}C$ and $\delta^{18}O$ records within the whole rostrum as long as minimally affected by diagenesis. Whether carbon and oxygen isotopes reflect physicochemical conditions of the belemnite habitat or whether vital effects are significant for either of the isotopic proxies cannot unequivocally be decided on the basis of the present data.

4.4.1 Carbon isotopes

Assuming that $\delta^{13}C$ values in the well-preserved parts represent the isotopic composition of dissolved inorganic carbon (DIC), short-term changes from +0.4 to +3.3 ‰ are recorded within the specimen. This range is in very good agreement with general observations on Early Toarcian specimens of the genus *Passaloteuthis* (**Fig. 1**, **Ullmann et al., 2014**) and may either reflect seasonal changes in DIC or belemnite migration through an isotopically heterogeneous water column. It has been noted, however, that $\delta^{13}C$ values of the best available extant belemnite analogue, the modern *Sepia*, show erratic $\delta^{13}C$ signatures that cannot easily be linked to environment (**Rexfort and Mutterlose, 2006, 2009**). Indeed, chemostratigraphic datasets using belemnite rostra show significant variability that may obscure isotopic excursions, unless abundant data are available and isotopic excursions are large (**Dera et al., 2011**; **Korte and Hesselbo, 2011**; **Ullmann et al., 2014**). Nevertheless, recognition of a perturbation in the carbon cycle using belemnite calcite appears to depend mostly on abundance of data, and in large datasets belemnite signals are found to be compatible with results for other fossil groups (**Wierzbowski and Joachimski, 2007**; **Korte and Hesselbo, 2011**; **Wierzbowski and Rogov, 2011**). Taxonomic differences or ecological changes seem only to play a major role in belemnite $\delta^{13}C$ records when extreme environmental perturbations are encountered (**Dera et al., 2011**; **Ullmann et al., 2014**).

4.4.2 Oxygen isotopes

Oxygen isotope ratios in biogenic calcite are a function of the isotopic composition of ambient water, its temperature and potential isotopic disequilibrium effects during calcite formation. No clear indication for a vital effect on belemnite $\delta^{18}O$ records has yet been reported and no significant depletions of ^{18}O related to vital effects are observed when comparing isotopic signatures of Jurassic belemnites to other coeval fossils (**Dera et al., 2011**; **Korte and Hesselbo, 2011**). It has been hypothesized that salinity changes could have had some bearing on elemental and isotopic heterogeneity of belemnite rostra (e.g. **Veizer, 1974**; **McArthur et al., 2007**; **Li et al., 2012, 2013**). For the Grey Shale Member (*Dactylioceras tenuicostatum* Subzone; **Fig. 1**), fully marine conditions without salinity variability have been inferred (**Sælen et al., 1996**). Strong salinity stratification of the European seaway (**Fig. 1**) has rather been put forward as one of the possible causes for the black shale formation of the later Early Toarcian Oceanic Anoxic Event (**Sælen et al., 1996**; **van de Schootbrugge et al., 2005**; **McArthur et al., 2008**). The $\delta^{18}O$ values of well-preserved samples of rostral calcite are therefore here taken to be a reliable

temperature proxy (see also **Urey et al., 1951**; **Bailey et al., 2003**; **Rexfort and Mutterlose, 2006**; **McArthur et al., 2007**; **Wierzbowski and Joachimski, 2007, 2009**; **Zakharov et al., 2011**; **Nunn and Price, 2010**; **Wierzbowski and Rogov, 2011**; **Li et al., 2012, 2013**; **Ullmann et al., 2014**). Excluding the zone around the apical line, $\delta^{18}O$ values remain comparatively heavy around -1.0 to -0.5 ‰ (**Fig. 10**) through the bulk of the rostrum. This range is in accordance with the average value observed for Early Toarcian specimens of the genus *Passaloteuthis* in the Cleveland Basin, Yorkshire, UK, from where the specimen originates (**Fig. 1**; **Sælen et al., 1996**; **McArthur et al., 2000**; **Li et al., 2012**; **Ullmann et al., 2014**). The $\delta^{18}O$ values in the outermost part of the rostrum decrease to ~ -2 ‰, indicating an increase in temperature recorded during that time in the life of the belemnite, possibly related to migration to slightly warmer waters. Coincident with the decreasing oxygen isotope ratios, $\delta^{13}C$ values increase, which is compatible with migration through a water column characterized by cooler deep water with relative ^{12}C enrichment in its DIC pool (**Ullmann et al., 2014**). Despite the range of oxygen isotope values observed here being in very good agreement with other data for *Passaloteuthis* sp. from the Cleveland Basin (**Sælen et al., 1996**; **Ullmann et al., 2014**), more rostra should be investigated to assess, whether similar isotopic profiles are observed for other examples of *Passaloteuthis* sp.

Critically, the juvenile stage of belemnite development can hardly ever be observed in geochemical proxies due to post-depositional alteration of the apical zone (**Podlaha et al., 1998**; **McArthur et al., 2000, 2007**; **Ullmann et al., 2013a**). Congruence between oxygen-isotope signatures in the juvenile part and the main body of the rostrum can be inferred from the very good linear fit of the regression line through the partially altered data of profile one (**Fig. 7**, $r^2 = 0.995$). If the growth bands representing the earliest life of the specimen carried significantly different $\delta^{13}C$ and $\delta^{18}O$ signatures, a reduction of the correlation coefficient and deviation from a binary mixing line compatible with the calcite cement would appear. It is therefore possible that the individual *P. bisulcata* studied here only formed growth increments capturing $\delta^{18}O$ values significantly lighter than -1 ‰ in the late life stage.

4.4.3 Sr/Ca ratios

The Sr/Ca ratios from the well-preserved parts of the belemnite, (1.39 to 2.20 mmol/mol, n = 324) agree very well with the range of Early Toarcian *Passaloteuthis* sp. 1.23 – 2.09 mmol/mol (n = 91; see Supplementary Information in **Ullmann et al., 2014**), and with belemnite data from the Early Toarcian *tenuicostatum* Zone in general (1.36 ± 0.36 mmol/mol; **Ullmann et al., 2013b**). A narrower range of Sr/Ca ratios (between 1.39 and 1.72 mmol/mol) results when taking only the well-preserved parts of the studied profiles into account and excluding the data of those parts showing pronounced bending of the calcite crystals (**Fig. 12**). This reduction of variability indicates that higher quality estimates for the chemical composition of seawater can be derived, when sampling of the central volume of the belemnite rostrum is avoid-

ed. The good match of Sr/Ca ratios and comparatively low variability measured for coeval *Passaloteuthis* sp. evidence that belemnite rostra are potentially very valuable archives for robust estimates of past seawater Sr/Ca ratios.

The potential for Sr/Ca ratios in belemnite calcite as a subsidiary proxy for palaeotemperature has been discussed previously with contrasting conclusions (**McArthur et al., 2000, 2007**; **Rosales et al., 2004a**; **Li et al., 2012, 2013**; **Ullmann et al., 2013b**). Our new data from the well-preserved parts of the fossil show a very weak correlation between Sr/Ca ratios and $\delta^{18}O$ values ($r^2 = 0.08$). This implies that the Sr/Ca ratios of *P. bisulcata* do not have a meaningful predictive value for estimating palaeotemperatures.

4.4.4 Mg/Ca ratios

Mg/Ca ratios of all well-preserved samples range from 6.8 to 18.1 mmol/mol. Values of >11.3 mmol/mol are eliminated from the dataset when samples of calcite from the central region showing curved morphologies are discounted (**Fig. 12**). These ranges compare to an observed variability of 7.5 to 14.1 mmol/mol in other Early Toarcian specimens of *Passaloteuthis* sp. (See Supplementary Information in **Ullmann et al., 2014**). Averages for all well-preserved samples observed in the present study (8.9 ± 2.8 mmol/mol; 2sd, n = 324) and in **Ullmann et al. (2014)** (9.8 ± 2.4 mmol/mol; 2sd, n = 91) agree within 10 % and show a similar spread of values. These observations indicate that Mg/Ca ratios in the genus *Passaloteuthis* are incorporated in a predictable way, which might eventually enable the reconstruction of seawater Mg/Ca using belemnite calcite. Due to missing modern analogues for the calcite rostrum proper (**Fuchs, 2012**), calibration of distribution coefficients, however, will only be possible by comparison with taxa for which closely related extant representatives can be studied.

Analogous to Sr/Ca ratios, Mg/Ca ratios in belemnite calcite have also been identified as a potential palaeotemperature proxy and also for this elemental ratio contrasting conclusions have been drawn (**McArthur et al., 2000, 2007**; **Rosales et al., 2004a**; **Li et al., 2012, 2013**). Our data for a single specimen show no significant correlation of Mg/Ca ratios with $\delta^{18}O$ values, suggesting that rather than temperature, factors such as metabolism, growth rate and crystal morphology are responsible for the variability observed in the calcite of this rostrum.

5 Conclusions

For the first time carbon and oxygen isotope data coupled with element/Ca ratios are presented for multiple, complete profiles through a single belemnite rostrum.

Diagenetic alteration is observed for the ventral margin of the rostrum and the central ~1.5 mm of the profiles, representing the apical line and immediate surroundings. Diagenetic trends are compatible with cementation of an originally porous (up to 40 % porosity) apical zone with isotopically depleted calcite.

Both, $\delta^{13}C$ and $\delta^{18}O$ values are uniform within ~0.5 ‰ in single growth bands and show systematic fluctuations along the geochemical profiles.

Mg/Ca and Sr/Ca ratios are strongly enriched in the well-preserved part of the central 4 mm of each profile (up to 70 % and 50 %, respectively). These enrichments are here linked to effects of crystal morphology.

Depletions of Mg and enrichments of Sr amounting to ~15 % in the profile closest to the apex with respect to the profile closest to the protoconch are related to enhanced rate of calcification towards the apex of the rostrum.

Residual systematic fluctuations of Mg/Ca and Sr/Ca throughout the rostrum probably represent metabolically controlled changes in the calcifying medium rather than changes in either temperature or the composition of ambient water.

The potential for the reconstruction of the elemental ratios of sea water in deep time from geochemical proxies in belemnite rostra is further documented.

REFERENCES

Al-Aasm I.S. and Veizer J. (1986a) Diagenetic stabilization of aragonite and low-Mg calcite, I. trace elements in rudists. J. Sediment. Petrol. 56, 138-152.

Al-Aasm I.S. and Veizer J. (1986b) Diagenetic stabilization of aragonite and low-Mg calcite, II. stable isotopes in rudists. J. Sediment. Petrol. 56, 763-770.

Bailey T.R., Rosenthal Y., McArthur J.M., van de Schootbrugge B. and Thirwall M.F. (2003) Paleoceanographic changes of the Late Pliensbachian-Early Toarcian interval: a possible link to the genesis of an Oceanic Anoxic Event. Earth Planet. Sci. Lett. 212, 307-320.

Barbin V. (2000) Cathodoluminescence of Carbonate Shells: Biochemical vs Diagenetic Process. In (eds. Pagel M., Barbin V., Blanc P., Ohnenstetter D.): Cathodoluminescence in Geosciences, Springer Berlin Heidelberg, 514 pp. doi: 10.1007/978-3-662-04086-7.

Benito M.I. and Reolid M. (2012) Belemnite taphonomy (Upper Jurassic, Western Tethys) part II: Fossil–diagenetic analysis including combined petrographic and geochemical techniques. Palaeogeogr. Palaeoclimatol. Palaeoecol. 358-360, 89-108.

Brand U. and Veizer J. (1980) Chemical diagenesis of a multicomponent carbonate system; 1, Trace elements. J. Sediment. Res. 50, 1219-1236. doi:10.1306/212F7BB7-2B24-11D7-8648000102-C1865D

Brand U. and Veizer J. (1981) Chemical diagenesis of a multicomponent carbonate system; 2, Stable isotopes. J.Sediment.Res.51,987-997.doi:10.1306/212F7DF6-

2B24-11D7-8648000102C1865D

Coleman M.L., Walsh J.N. and Benmore R.A. (1989) Determination of both chemical and stable isotope composition in milligramme-size carbonate samples. Sediment. Geol. 65, 233-238. doi:10.1016/0037-0738(89)90025-0

Coward M.P., Dewey J.F., Hempton M. and Holroyd J. (2003) Tectonic evolution, in (eds. Evans, D., et al.), The millennium atlas: Petroleum geology of the central and northern North Sea: London, Geological Society Publishing House, p. 17-33.

DePaolo D.J. (2011) Surface kinetic model for isotopic and trace element fractionation during precipitation of calcite from aqueous solutions. Geochim. Cosmochim. Acta 75, 1039-1056. doi:10.1016/j.gca.2010.11.020

Dera G., Brigaud B., Monna F., Laffont R., Pucéat E., Deconinck J.-F., Pellenard P., Joachimski M.M. and Durlet C. (2011) Climatic ups and downs in a disturbed Jurassic world. Geology 39, 215-218. doi:10.1130/G31579.1

Doyle P. (1990) The British Toarcian (Lower Jurassic) belemnites Part I, Monograph of the Palaeontographical Society. London.

Dutton A., Huber B.T., Lohmann K.C. and Zinsmeister W.J. (2007) High-resolution stable isotope profiles of a dimitobelid belemnite: Implications for paleodepth habitat and late Maastrichtian climate seasonality. Palaios 22, 642-650.

Fuchs D. (2012) The "rostrum"-problem in coleoid terminology – an attempt to clarify inconsistencies. Geobios 45, 29-39. doi:10.1016/j.geobios.2011.11.014

Gabitov R.I., Sadekov A. and Leinweber A. (2014) Crystal growth rate effect on Mg/Ca and Sr/Ca partitioning between calcite and fluid: An in situ approach. Chemical Geology 367, 70-82.

Hesselbo S.P. and Jenkyns H.C. (1995) A comparison of the Hettangian to Bajocian successions of Dorset and Yorkshire, in: Field Geology of the British Jurassic. Geological Society, London, London, pp. 105-150.

Imai N., Terashima S., Itoh S. and Ando A. (1996) 1996 Compilation of analytical data on nine GSJ geochemical reference samples, "sedimentary rock series." Geostand. Newsl. 20, 165-216. doi:10.1111/j.1751-908X.1996.tb00184.x

Korte C. and Hesselbo S.P. (2011) Shallow marine carbon and oxygen isotope and elemental records indicate icehouse-greenhouse cycles during the Early Jurassic. Paleoceanography 26, PA4219. doi:10.1029/2011PA002160

Li Q., McArthur J.M. and Atkinson T.C. (2012) Lower Jurassic belemnites as indicators of palaeo-temperature. Palaeogeogr. Palaeoclimatol. Palaeoecol. 315-316, 38-45. doi:10.1016/j.palaeo.2011.11.006

Li Q., McArthur J.M., Doyle P., Janssen N., Leng M.J., Müller W. and Reboulet S. (2013) Evaluating Mg/Ca in belemnite calcite as a palaeo-proxy. Palaeogeogr. Palaeoclimatol. Palaeoecol. 388, 98-108. doi:10.1016/j.palaeo.2013.07.030

Longinelli A. (1969) Oxygen-18 variations in belemnite guards. Earth Planet. Sci. Lett. 7, 209-212. doi:10.1016/0012-821X(69)90038-7

Machel H.G. (1985) Cathodoluminescence in calcite and dolomite and its chemical interpretation. Geoscience Canada 12 (4), 139-147.

McArthur J.M., Donovan D., Thirlwall M.F., Fouke B.W. and Mattey D. (2000) Strontium isotope profile of the early Toarcian (Jurassic) oceanic anoxic event, the duration of ammonite biozones, and belemnite palaeotemperatures. Earth Planet. Sci. Lett. 179, 269-285. doi:10.1016/S0012-821X(00)00111-4

McArthur J.M., Doyle P., Leng M.J., Reeves K., Williams C.T., Garcia-Sanchez R. and Howarth R.J. (2007) Testing palaeo-environmental proxies in Jurassic belemnites: Mg/Ca, Sr/Ca, Na/Ca, δ18O and δ13C. Palaeogeogr. Palaeoclimatol. Palaeoecol. 252, 464-480. doi:10.1016/j.palaeo.2007.05.006

McArthur J.M., Algeo T.J., van de Schootbrugge B., Li Q. and Howarth R.J. (2008) Basinal restriction, black shales, Re-Os dating, nd the Early Toarcian (Jurassic) oceanic anoxic event. Paleoceanography 23, PA4217. doi: 10.1029/2008PA001607

Morse J.W. and Bender M.L. (1990) Partition coefficients in calcite: Examination of factors influencing the validity of experimental results and their application to natural systems. Chem. Geol. 82, 265-277. doi:10.1016/0009-2541(90)90085-L

Nunn E.V. and Price G.D. (2010) Late Jurassic (Kimmeridgian–Tithonian) stable isotopes (δ18O, δ13C) and Mg/Ca ratios: New palaeoclimate data from Helmsdale, northeast Scotland. Palaeogeogr. Palaeoclimatol. Palaeoecol. 292, 325-335. doi:10.1016/j.palaeo.2010.04.015

Podlaha O.G., Mutterlose J. and Veizer J. (1998) Preservation of δ18O and δ13C in belemnite rostra from the Jurassic/Early Cretaceous successions. Am. J. Sci. 298, 324-347.

Price G.D. and Passey B.H. (2013) Dynamic polar climates in a greenhouse world: Evidence from clumped isotope thermometry of Early Cretaceous belemnites. Geology 41, 923-926.

Price G.D. and Rogov M.A. (2009) An isotopic appraisal of the Late Jurassic greenhouse phase in the Russian Platform. Palaeogeogr. Palaeoclimatol. Palaeoecol. 273, 41-49. doi:10.1016/j.palaeo.2008.11.011

Rexfort A. and Mutterlose J. (2006) Stable isotope records from Sepia officinalis—a key to understanding the ecology of belemnites? Earth Planet. Sci. Lett. 247, 212-221. doi:10.1016/j.epsl.2006.04.025

Rexfort A. and Mutterlose J. (2009) The role of biogeography and ecology on the isotope signature of cuttlefishes (Cephalopoda, Sepiidae) and the impact on belemnite studies. Palaeogeogr. Palaeoclimatol. Palaeoecol. 284, 153-163. doi:10.1016/j.palaeo.2009.09.021

Richter D.K., Neuser R.D., Schreuer J., Gies H. and Immenhauser A. (2011) Radiaxial-fibrous calcites: A new look at an old problem. Sediment. Geol. 239, 23-36. doi:10.1016/j.sedgeo.2011.06.003

Rimstidt J.D., Balog A. and Webb J. (1998) Distribution of trace elements between carbonate minerals and aqueous solutions. Geochim. Cosmochim. Acta 62, 1851-1863. doi:10.1016/S0016-7037(98)00125-2

Rosales I., Quesada S. and Robles S. (2004a) Paleo-

temperature variations of Early Jurassic seawater recorded in geochemical trends of belemnites from the Basque–Cantabrian basin, northern Spain. Palaeogeogr. Palaeoclimatol. Palaeoecol. 203, 253-275. doi:10.1016/S0031-0182(03)00686-2

Rosales I., Robles S. and Quesada S. (2004b) Elemental and Oxygen Isotope Composition of Early Jurassic Belemnites: Salinity vs. Temperature Signals. J. Sediment. Res. 74, 342-354.

Sælen G. (1989) Diagenesis and construction of the belemnite rostrum. Palaeontology 32, 765-798.

Sælen G., Doyle P. and Talbot M.R. (1996) Stable-isotope analyses of belemnite rostra from the Whitby Mudstone Fm., England: Surface water conditions during deposition of a marine black shale. Palaios 11, 97-117. doi:10.2307/3515065

Spaeth C. (1975) Zur Frage der Schwimmverhältnisse bei Belemniten in Abhängigkeit vom Primärgefüge der Hartteile. Paläontologische Zeitschrift 49, 321-331.

Spötl C. and Vennemann T.W. (2003) Continuous-flow isotope ratio mass spectrometric analysis of carbonate minerals. Rapid Commun. Mass Spectrom. 17, 1004-1006. doi:10.1002/rcm.1010

Stevens G.R. and Clayton R.N. (1971) Oxygen isotope studies on Jurassic and Cretaceous belemnites from New Zealand and their biogeographic significance. N. Z. J. Geol. Geophys. 14, 829-897. doi:10.1080/00288306.1971.10426336

Ullmann C.V. and Korte C. (2015) Diagenetic alteration in low-Mg calcite from macrofossils: a review. Geological Quarterly 59 (1), 3-20.

Ullmann C.V., Campbell H.J., Frei R., Hesselbo S.P., Pogge von Strandmann P.A.E. and Korte C. (2013a) Partial diagenetic overprint of Late Jurassic belemnites from New Zealand: Implications for the preservation potential of δ^7Li values in calcite fossils. Geochim. Cosmochim. Acta 120, 80-96. doi:10.1016/j.gca.2013.06.029

Ullmann C.V., Hesselbo S.P. and Korte C. (2013b) Tectonic forcing of Early to Middle Jurassic seawater Sr/Ca. Geology 41, 1211-1214. doi:10.1130/G34817.1

Ullmann C.V., Thibault N., Ruhl M., Hesselbo S.P. and Korte C. (2014) Effect of a Jurassic oceanic anoxic event on belemnite ecology and evolution. Proc.

Natl. Acad. Sci. 111, 10073-10076. doi:10.1073/pnas.1320156111

Urey H.C., Lowenstam H.A., Epstein S. and McKinney C.R. (1951) Measurement of paleotemperatures and temperatures of the Upper Cretaceous of England, Denmark, and the Southeastern United States. Geol. Soc. Am. Bull. 62, 399-416. doi:10.1130/0016-7606-(1951)62[399:MOPATO]2.0.CO;2

van de Schootbrugge B., McArthur J.M., Bailey T.R., Rosenthal Y., Wright J.D. and Miller K.G. (2005) Toarcian oceanic anoxic event: An assessment of global causes using belmnite C isotope records. Paleoceanography 20, PA3008. doi: 10.1029/2004PA001102

Veizer J. (1974) Chemical diagenesis of belemnite shells and possible consequences for paleotemperature determinations. Neues Jahrb. Für Geol. Paläontol. Abh. 147, 91-111.

Wierzbowski H. (2013) Life span and growth rate of Middle Jurassic mesohibolitid belemnites deduced from rostrum microincrements. Vol. Jurassica 11, 1-18.

Wierzbowski H. and Joachimski M. (2007) Reconstruction of late Bajocian–Bathonian marine palaeoenvironments using carbon and oxygen isotope ratios of calcareous fossils from the Polish Jura Chain (central Poland). Palaeogeogr. Palaeoclimatol. Palaeoecol. 254, 523-540. doi:10.1016/j.palaeo.2007.07.010

Wierzbowski H. and Joachimski M.M. (2009) Stable isotopes, elemental distribution, and growth rings of belemnopsid belemnite rostra: proxies for belemnite life habitat. Palaios 24, 377-386. doi:10.2110/palo.2008.p08-101r

Wierzbowski H. and Rogov M. (2011) Reconstructing the palaeoenvironment of the Middle Russian Sea during the Middle–Late Jurassic transition using stable isotope ratios of cephalopod shells and variations in faunal assemblages. Palaeogeogr. Palaeoclimatol. Palaeoecol. 299, 250–264. doi:10.1016/j.palaeo.2010.11.006

Zakharov Y.D., Shigeta Y., Nagendra R., Safronov P.P., Smyshlyaeva O.P., Popov A.M., Velivetskaya T.A. and Afanasyeva T.B. (2011) Cretaceous climate oscillations in the southern palaeolatitudes: New stable isotope evidence from India and Madagascar. Proc. 8th Int. Symp. Cretac. Syst. 32, 623-645. doi:10.1016/j.cretres.2011.04.007